Acta Mech 226, 3243–3261 (2015)
DOI 10.1007/s00707-015-1377-4

ORIGINAL PAPER

Xiaoguang Yuan · Lei Li

Wave reflection and refraction in rotating and initially-stressed piezoelectric crystals

Received: 27 November 2014 / Revised: 18 March 2015 / Published online: 22 May 2015

Abstract The purpose of this paper is to address the wave reflection and refraction in the rotating piezoelectric crystals subjected to a biaxial, homogeneous stress field. Besides, utilizing the inhomogeneous wave theory enables additional reflected and refracted surface waves to solve the problem of discrepancy between independent wave modes and boundary equations. A set of homogeneous equations in displacements and electric potential is derived within the rotatory coordinate system in the presence of the Coriolis and centrifugal acceleration. The performed plane example shows that there is a critical point when angular velocity equals the wave frequency, at which no quasi-longitudinal wave can be generated, reflected or refracted, and close to which the characteristics of the quasi-longitudinal wave change sharply. In addition, the presence of the Coriolis and centrifugal accelerations demonstrates noticeable influence upon the wave propagation and reflection/refraction, namely the wave velocities and attenuations, the angles of the reflected/refracted bulk waves, the reflection/refraction amplitudes and energy ratio coefficients. The analysis results also indicate that the reflected and refracted waves can transform into the type of surface wave at some incident angles. Finally, compared with the rotation effects, the waves are not sensitive to the initial stresses.

1 Introduction

Piezoelectrics are the most common transducers in the engineering field used in the rotary environment. For instance, the gyroscopes of rotating motion sensors have important applications in automobiles, video cameras, smart weapon systems, machine control, robotics and navigation. Piezoelectric gyroscopes can make use of rotation-induced frequency shifts in surface acoustic wave (SAW) or bulk acoustic wave (BAW) piezoelectric resonators to measure angular rates. On the other hand, due to the nonuniform material properties, coefficients of thermal expansion and chemical/nucleation shrinkage/growth during the manufacture processing and cool down to operating or room temperature, the presence of initial stress is unavoidable. Also, to improve performance or select suitable operating conditions of SAW devices, such as selection of filters, stability of oscillators and temperature compensation, the generalized displacements or stresses are applied to establish a biasing state. Thus, it is necessary to learn the effects of rotation and initial stresses on the piezoelectric wave propagation, reflection and refraction.

As far as we know, the research of rotation-affected vibrations or waves was started by Huston [1] who investigated the effect of "rigid-body" rotation on wave propagation velocities in elastic media. Later, the rotation effect was studied in the "in-plane" vibration of rotating circular disks [2]. It was found that the

X. Yuan (✉)
School of Civil Engineering, Henan Polytechnic University, Jiaozuo 454000, People's Republic of China
E-mail: xgyuan@gmail.com

L. Li
School of Material Science and Engineering, Henan Polytechnic University, Jiaozuo 454000, People's Republic of China

inclusion of Coriolis and centripetal accelerations leads to the result that the medium becomes dispersive and anisotropic [3]. Lao [4] derived the effect of rotation on surface acoustic waves in a perturbation treatment of the Coriolis force for an isotropic medium. Chaudhuri and Debnath [5] obtained a more general dispersion relation to determine the effects of rotation, relaxation time and the external magnetic field on the phase velocity of the waves. The problem of wave propagation in a rotating random infinite magneto-thermo-visco-elastic medium was studied, and a coupled dispersion relation for longitudinal and transverse waves was deduced to determine the effect of viscoelasticity, relaxation times and rotation on the phase velocity of the coupled waves [6]. In the work of Wauer [7], the propagation of waves in a conducting piezoelectric solid was studied for the case when the entire medium rotates with a uniform angular velocity. Destrade and Saccomandi [8] raised and addressed two questions related to elastic motions and found some finite amplitude transverse waves in rotating incompressible elastic solids with general shear response. Destrade [9] studied the propagation of surface (Rayleigh) waves over a rotating orthorhombic crystal, in which the secular equation for the surface wave speed was found explicitly. In the work of Ting [10], the Stroh formalism for surface waves in an anisotropic elastic half-space was extended to the case when the half-space rotates about an axis with a constant rotation rate. Auriault [11] revealed that the free wave propagation in non-Galilean rotating media gives rise to two dispersive waves, which are coupled dilatational–shear waves. Moreover, Auriault [12] investigated wave propagation in elastic porous media which are saturated by incompressible viscous Newtonian fluids when the porous media are in rotation with respect to a Galilean frame. Yang [13] presented a review of analyses on vibrations of rotating piezoelectric structures for applications in piezoelectric angular rate sensors. Propagation of plane waves in a micropolar porous elastic solid rotating with a uniform angular velocity was investigated in [14]. Sharma and Grover [15] dealt with the propagation of body waves in a rotating, generalized thermoelastic solid by using Cardano's and perturbation methods. Kumar and Rupender [16] solved a two-dimensional problem in an electromagnetic micropolar generalized thermoelastic medium subjected to mechanical forces or thermal sources. Biryukov et al. [17] investigated the gyroscopic effect in arbitrary crystals by taking into account the medium rotation. Recently, Sharma et al. [18] considered the propagation of body waves in a homogenous isotropic, rotating and generalized thermoelastic solid with voids. Wegert et al. [19] analyzed theoretical upper bounds for the size of the gyroscopic effect on the frequency of guided acoustic waves in (piezo-)elastic media, which are valid in the regime of small rotation rates as compared to the frequency of the guided acoustic wave. Prasad and Mukhopadhyay [20] aimed at the effects of rotation on the propagation of harmonic plane waves under two-temperature thermoelasticity theory. Kothari and Mukhopadhyay [21] analyzed the effects of rotation on the propagation of harmonic plane waves in an unbounded thermoelastic medium rotating with a uniform angular velocity. Abd-Alla and Yahya [22] investigated the effect of rotation on an infinite circular cylinder subjected to certain boundary conditions. The author [23] established an analysis of an inhomogeneous wave in the rotating piezoelectric body. Yuan and Chen [24] presented an analysis on the effect of rotation upon surface acoustic waves propagating in a piezoelectric half-space. Yuan [25] addressed the wave reflection over the rotating piezoelectric boundary surface in the framework of inhomogeneous wave. Taking account of initial stresses, Pao and Gamer [26] formulated the acoustoelasticity equations to investigate the propagation of ultrasonic waves in orthotropic elastic solids. Simionescu-Panait [27] investigated the problem of propagation of Love-type waves in a prestressed anisotropic layered structure. Gandhi et al. [28] considered the effect of stress on Lamb waves apropagating in a homogeneous and initially isotropic plate subjected to a homogeneous biaxial stress field. In the chapter 6 of Kuang's book [29], the motion equations accounting for the initial displacements or stresses are derived in detail, and Love-wave theory in such structure is established.

As stated above, it is seen that many achievements have been done on the rotation effects on waves. To our knowledge, no systematic research exists addressing the question of inhomogeneous wave reflection and refraction over the boundary interface accounting for rotation and initial stresses. This paper aims to further this study by considering two bonded rotating and biaxially stressed piezoelectric crystals with the inhomogeneous wave theory [30–33].

The paper is organized in the following manner. In the next section, the basic equations for motion in presence of the Coriolis and centrifugal accelerations are established as well as the corresponding half plane boundary. Next, utilizing the inhomogeneous wave theory, we recast the dispersion equations in a general complex form that admits separable real solutions to define the phase velocity and attenuation. Further, the boundary solution will be obtained in the following content. Finally, the numerical results and discussions of the plane problem are presented and conclusions are inferred, respectively.

2 Basic governing equations

2.1 The equation of motion

Let us define two frames $\Re$ and $\Re'$ in relative motion as shown in Fig. 1. The frame $\Re$ is inertial, with origin at the center o, and whose axes are along directions of base vector $\mathbf{e}_1, \mathbf{e}_2, \mathbf{e}_3$. The frame $\Re'$ is originated at O, and the base vectors of its axes are $\mathbf{E_1}, \mathbf{E_2}, \mathbf{E_3}$. The piezoelectric body is fastened to $\Re'$, which rotates about $\Re$ with angular velocity $\mathbf{\Omega}$. The following relations of a point M in the piezoelectric body $a_{\Re}(M)$ in $\Re$ and $a_{\Re'}(M)$in $\Re'$ may easily be obtained [34],

$$a_{\Re}(\mathbf{r}_M) = a_{\Re'}(\boldsymbol{\rho}_M) + 2\Omega \wedge v_{\Re'}(\boldsymbol{\rho}_M) + \Omega \wedge (\Omega \wedge \boldsymbol{\rho}_M) + \frac{\mathrm{d}^2\mathbf{r}_0}{\mathrm{d}t^2}$$
$$\Omega = \Omega_1\mathbf{e}_1 + \Omega_2\mathbf{e}_2 + \Omega_3\mathbf{e}_3, \tag{1}$$

in which the term $\mathbf{r}_M$ is the position vector in frame $\Re$, $\boldsymbol{\rho}_M$ is the position vector in frame $\Re'$, $\mathbf{r}_0$ is the vector from origin o to O, $2\Omega \wedge v_{\Re'}(\boldsymbol{\rho}_M)$ is the Coriolis acceleration, $a_{\Re'}(\boldsymbol{\rho}_M)$ is the acceleration of M in the viewpoint of frame $\Re'$, Ω is the angular velocity of frame $\Re'$ relative to the frame $\Re$, and $\Omega \wedge (\Omega \wedge \boldsymbol{\rho}_M)$ is the centrifugal acceleration. If the origin O stays fixed, $\frac{\mathrm{d}^2\mathbf{r}_0}{\mathrm{d}t^2}$ is equal to zero.

The momentum balance equation takes into account the above rotation-related terms and reads

$$\rho\left[\frac{\partial^2\mathbf{u}_{\Re'}}{\partial t^2} + 2\Omega \wedge \frac{\partial\mathbf{u}_{\Re'}}{\partial t} + \Omega \wedge (\Omega \wedge (\mathbf{x} + \mathbf{u}_{\Re'}))\right] = \nabla \cdot \boldsymbol{\sigma}. \tag{2}$$

In the above equation, ρ is the mass density, t is the time variable, $\mathbf{x}$ is the position vector of M, $\mathbf{u}_{\Re'}$ is the displacement vector (hereafter we will use $\mathbf{u}$ for clarity), $\boldsymbol{\sigma}$ is the Cauchy stress tensor, ε_{jik} is the permutation tensor, and the subscripts range from 1 to 3.

Equivalently, Eq. (2) can be written in the component form

$$\rho\left[\frac{\partial^2 u_j}{\partial t^2} + \varepsilon_{jik}\varepsilon_{kmn}\Omega_i\Omega_m(u_n + x_n) + 2\varepsilon_{jik}\Omega_i\frac{\partial u_k}{\partial t}\right] = \sigma_{ij,i}. \tag{3}$$

Further, the electric field can be described by the electrostatic equation

$$D_{i,i} = 0 \tag{4}$$

where D_i is the electric displacement vector and the Einstein summation convention is implied.

The following material equations are employed:

$$\sigma_{ij} = \overset{\mathrm{o}}{C}_{ijkl}\,\varepsilon_{kl} - e_{kij}E_k,$$
$$D_i = \in_{ij} E_j + e_{ikl}\varepsilon_{kl} \tag{5}$$

where ε_{ij} are the strain and E_k the electric field vector, while $\overset{\mathrm{o}}{C}_{ijkl}$, e_{kij} and $\in_{ij}$ are the instantaneous elasticity tensor, piezoelectricity and permittivity tensors of the material.

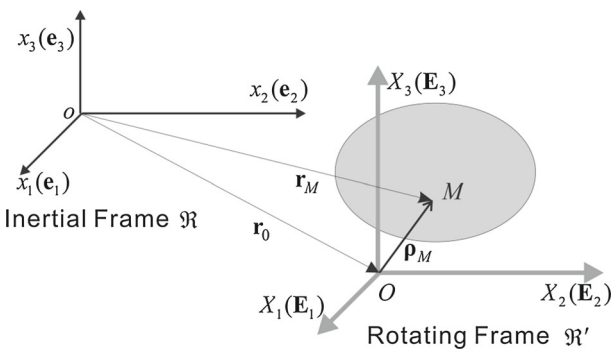

Fig. 1 Rotating piezoelectric body

The instantaneous elasticity tensor can be expressed in terms of the classical moduli of the material and on the initial applied field as follows [26,27,29]:

$$\overset{\circ}{C}_{ijkl} = C_{ijkl} + \delta_{kj}\sigma^0_{il} \tag{6}$$

where σ^0_{il} are the components of the initial applied symmetric (Cauchy) stress tensor.

Quasi-statically, the electric field vector can be derived from an electric potential, that is,

$$E_k = -\varphi_{,k} \tag{7}$$

in which φ is the electric potential.

The geometric relationship between the strain and the displacement tensors is defined as

$$\varepsilon_{kl} = \frac{1}{2}\left(u_{k,l} + u_{l,k}\right). \tag{8}$$

Eliminating ε_{kl} and E_k from Eqs. (5), (7) and (8) yields

$$\begin{aligned} \sigma_{ij} &= \overset{\circ}{C}_{ijkl}u_{k,l} + e_{kij}\varphi_{,k}, \\ D_i &= -\in_{ij}\varphi_{,j} + e_{ikl}u_{k,l}. \end{aligned} \tag{9}$$

Then, inserting Eq. (9) into Eqs. (3) and (4) leads to a set of wave equations for a rotating piezoelectric body,

$$\begin{aligned} \rho\left[\frac{\partial^2 u_j}{\partial t^2} + \varepsilon_{jik}\varepsilon_{kmn}\Omega_i\Omega_m u_n + 2\varepsilon_{jik}\Omega_i\frac{\partial u_k}{\partial t}\right] - \overset{\circ}{C}_{ijkl}u_{k,li} - e_{kij}\varphi_{,ki} &= -\rho\varepsilon_{jik}\varepsilon_{kmn}\Omega_i\Omega_m x_n \\ -\in_{ij}\varphi_{,ji} + e_{ikl}u_{k,li} &= 0, \end{aligned} \tag{10}$$

by which the homogeneous equations of motion in the displacement u_{i} and electric potential φ are formulated as

$$\begin{aligned} \rho\left[\frac{\partial^2 u_j}{\partial t^2} + \varepsilon_{jik}\varepsilon_{kmn}\Omega_i\Omega_m u_n + 2\varepsilon_{jik}\Omega_i\frac{\partial u_k}{\partial t}\right] - \overset{\circ}{C}_{ijkl}u_{k,li} - e_{kij}\varphi_{,ki} - (u_{j,k}\sigma^0_{ki})_{,i} &= 0 \\ -\in_{ij}\varphi_{,ji} + e_{ikl}u_{k,li} &= 0 \end{aligned} \tag{11}$$

which contains four equations (three elastic wave equations and one electric wave equation that is associated with the elastic waves by the material relationship Eq. (5) and three independent unknown variables: u_1, u_2, u_3 and φ).

2.2 Two-dimensional case

For easily handling the boundary condition and governing equations, in this paper, it is preferable to define all the equations in the rotating $\Re'$ frame. Thus, any quantities involving the base vectors $\mathbf{e}_1$, $\mathbf{e}_2$, $\mathbf{e}_3$ like the angular velocity can be converted into $\mathbf{E_1}$, $\mathbf{E_2}$, $\mathbf{E_3}$, and the components of $\mathbf{\Omega}$ in the $\Re'$ frame can be obtained. Finally, all the functions like $\mathbf{u}$, φ, $\mathbf{\Omega}$ in Eq. (11) should also be expressed with the same coordinates X_1, X_2, X_3, t.

As the case of the half plane problem, assuming the origins of inertial and rotating frame is coincident, thus X_1X_2 and x_1x_2 are parallel, and the piezoelectric plane is rotating about X_3 with the angular velocity $\mathbf{\Omega} = \Omega_3\mathbf{E_3}$; consequently, Eq. (11) takes the form

$$\begin{aligned} \rho\left[\frac{\partial^2 u_1}{\partial t^2} - \Omega_3^2 u_1 - 2\Omega_3\frac{\partial u_2}{\partial t}\right] - \overset{\circ}{C}_{i1kl}u_{k,li} - e_{ki1}\varphi_{,ki} &= 0, \\ \rho\left[\frac{\partial^2 u_2}{\partial t^2} - \Omega_3^2 u_2 + 2\Omega_3\frac{\partial u_1}{\partial t}\right] - \overset{\circ}{C}_{i2kl}u_{k,li} - e_{ki2}\varphi_{,ki} &= 0 \\ -\in_{ij}\varphi_{,ji} + e_{ikl}u_{k,li} &= 0, \end{aligned} \tag{12}$$

which are the governing equations of the rotating half plane problem accompanied by the boundary condition of Eq. (23).

2.3 The inhomogeneous wave solution

Generally, the wave equations of Eq. (11) or (12) can be solved by introducing the complex monochromatic plane wave functions,

$$\begin{aligned} u_i &= U_i e^{I(k_j x_j - \omega t)}, \\ \varphi &= \Psi e^{I(k_j x_j - \omega t)} \end{aligned} \tag{13}$$

where k_j is the complex wave vector, ω is the wave circular frequency, I is the imaginary unit equal to $\sqrt{-1}$, t is the time variable, and $(U_i,\ \Psi)$ are the complex amplitudes of displacements and electric potential, respectively. Inserting Eq. (13) into (10) gives

$$\begin{aligned} \rho\omega^2\left[-U_j + \varepsilon_{jik}\varepsilon_{kmn}\frac{\Omega_i}{\omega}\frac{\Omega_m}{\omega}U_n - 2I\varepsilon_{jik}\frac{\Omega_i}{\omega}U_k\right] + \overset{\circ}{C}_{ijkl}k_l k_i U_k + e_{kij}k_k k_i \Psi = 0 \\ \in_{ij} k_j k_i \Psi - e_{ikl}U_k k_l k_i = 0. \end{aligned} \tag{14}$$

A nontrivial solution of these four linear homogeneous equations for U_1, U_2, U_3, Ψ exists only if the determinant of the coefficients vanishes, which yields the governing dispersion relation

$$\det \mathbf{G} = 0 \tag{15}$$

in which the elements g_{ij} $(i,\ j = 1, 2, 3, 4)$ of the matrix $\mathbf{G}$ are

$$\begin{bmatrix} g_{11} & g_{12} & g_{13} & g_{14} \\ g_{21} & g_{22} & g_{23} & g_{24} \\ g_{31} & g_{32} & g_{33} & g_{34} \\ g_{41} & g_{42} & g_{43} & g_{44} \end{bmatrix} \begin{Bmatrix} U_1 \\ U_2 \\ U_3 \\ \Psi \end{Bmatrix} = \begin{Bmatrix} 0 \\ 0 \\ 0 \\ 0 \end{Bmatrix} \tag{16}$$

where

$$\begin{aligned} g_{1s} &= \rho\omega^2\left[-\delta_{1s} + \varepsilon_{1ik}\varepsilon_{kms}\frac{\Omega_i}{\omega}\frac{\Omega_m}{\omega} - 2I\varepsilon_{1is}\frac{\Omega_i}{\omega}\right] + \overset{\circ}{C}_{i1sl}k_l k_i, \quad s = 1, 2, 3, \\ g_{14} &= e_{ki1}k_k k_i \Psi, \\ g_{2s} &= \rho\omega^2\left[-\delta_{2s} + \varepsilon_{2ik}\varepsilon_{kms}\frac{\Omega_i}{\omega}\frac{\Omega_m}{\omega} - 2I\varepsilon_{2is}\frac{\Omega_i}{\omega}\right] + \overset{\circ}{C}_{i2sl}k_l k_i, \quad s = 1, 2, 3, \\ g_{24} &= e_{ki2}k_k k_i \Psi, \\ g_{3s} &= \rho\omega^2\left[-\delta_{3s} + \varepsilon_{3ik}\varepsilon_{kms}\frac{\Omega_i}{\omega}\frac{\Omega_m}{\omega} - 2I\varepsilon_{3is}\frac{\Omega_i}{\omega}\right] + \overset{\circ}{C}_{i3sl}k_l k_i, \quad s = 1, 2, 3, \\ g_{34} &= e_{ki3}k_k k_i \Psi, \\ g_{41} &= -e_{i1l}k_l k_i,\ g_{42} = -e_{i2l}k_l k_i\, g_{43} = -e_{i3l}k_l k_i,\ g_{44} = \in_{ij} k_j k_i. \end{aligned} \tag{17}$$

In the case of the plane problem, inserting Eq. (13) into Eq. (12) gives

$$\begin{bmatrix} \Gamma_{11} - \rho(\omega^2 + \Omega_3^2) & \Gamma_{12} + 2\rho I\omega\Omega_3 & e_1^* \\ \Gamma_{21} - 2\rho I\omega\Omega_3 & \Gamma_{22} - \rho(\omega^2 + \Omega_3^2) & e_2^* \\ e_1^* & e_2^* & -\in^* \end{bmatrix} \begin{Bmatrix} U_1 \\ U_2 \\ \Psi \end{Bmatrix} = \begin{Bmatrix} 0 \\ 0 \\ 0 \end{Bmatrix} \tag{18}$$

where

$$\Gamma_{ik} = \overset{\circ}{C}_{ijkl}k_j k_l, \quad e_i^* = e_{kij}k_k k_j, \quad \in^* = \in_{jk} k_k k_j.$$

The existence of nontrivial solutions of Eq. (18) requires its corresponding characteristic equation to be equal to zero, that is the dispersion equation

$$\det\begin{bmatrix} \Gamma_{11} - \rho(\omega^2 + \Omega_3^2) & \Gamma_{12} + 2\rho I\omega\Omega_3 & e_1^* \\ \Gamma_{21} - 2\rho I\omega\Omega_3 & \Gamma_{22} - \rho(\omega^2 + \Omega_3^2) & e_2^* \\ e_1^* & e_2^* & -\in^* \end{bmatrix} = 0. \tag{19}$$

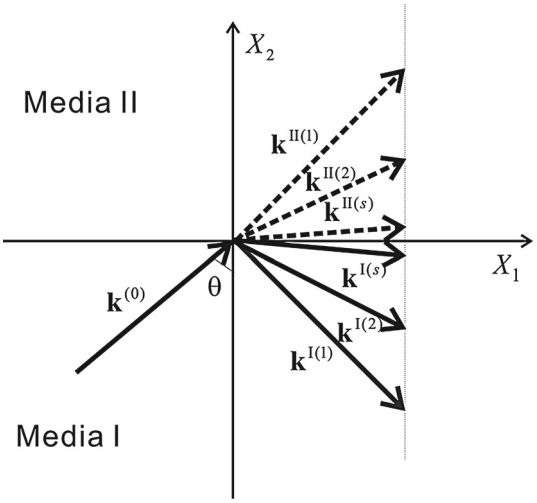

Fig. 2 Illustrations of wave vectors in reflection problem in $X_1 - X_2$ plane. $k^{(0)}$ is the incident wave, and $k^{I(1)}...k^{I(s)}$ are the wave vectors of the reflected wave modes, and $k^{II(1)}...k^{II(s)}$ are the wave vectors of the refracted wave modes

Further, the inhomogeneous wave theory [30,32] allows the complex wave vector to be decomposed in terms of the wave propagation direction as

$$k_j = P_j + IA_j = Pn_j + IAm_j \tag{20}$$

where P_j is the propagation vector with its magnitude of $P = \sqrt{P_j P_j}$, and A_j is the attenuation vector with its magnitude of $A = \sqrt{A_j A_j}$. And the unit vectors (n_j, m_j) can be expressed in terms of the angle θ between n_j and X_2, and the attenuation angle γ between n_j and m_j as shown in Fig. 2. Via Eq. (20), we obtain

$$\begin{aligned} \{n_1, n_2\} &= \{\sin\theta, \cos\theta\}^T, \\ \{m_1, m_2\} &= \{\sin(\theta+\gamma), \cos(\theta+\gamma)\}^T, \\ n_j m_j &= \cos\gamma. \end{aligned} \tag{21}$$

Inserting Eq. (20) into the dispersion equation, we can obtain P and A, and thus, the wave phase velocity can be defined as

$$c_p = \frac{\omega}{P}, \tag{22}$$

and A is the corresponding wave attenuation.

3 The reflection/refraction waves over the interface between two piezoelectric materials

In the case of ideal contact, the boundary conditions for the stress tensor are reduced to the requirements for the continuity of the interface tractions and displacement vectors along the interface between the two piezoelectric crystals, respectively.

The boundary conditions at stress-free and electrically shorted/charge-free surface are

$$\begin{aligned} \left(\boldsymbol{\sigma}^{(\mathrm{I})} - \boldsymbol{\sigma}^{(\mathrm{II})}\right) \cdot \mathbf{N} &= \mathbf{0}, \\ \mathbf{u}^{(\mathrm{I})} &= \mathbf{u}^{(\mathrm{II})} \end{aligned} \tag{23}$$

where $\mathbf{N}$ is the unit direction vector of the boundary surface, and apparently, it will not change its form in the $\Re'$ frame. Alternatively, for a rotating body in the inertial $\Re$ frame, this direction vector is associated with the angular velocity $\boldsymbol{\Omega}$ by

$$\mathbf{n} = \frac{\boldsymbol{\Omega} \wedge \mathbf{N}}{\|\boldsymbol{\Omega} \wedge \mathbf{N}\|}. \tag{24}$$

Thus, the boundary condition (23) can also be formulated in the inertial $\Re$ frame, which is

$$\begin{aligned}\left(\boldsymbol{\sigma}^{(\mathrm{I})}-\boldsymbol{\sigma}^{(\mathrm{II})}\right)\cdot\mathbf{n}&=\mathbf{0},\\ \mathbf{u}^{(\mathrm{I})}&=\mathbf{u}^{(\mathrm{II})}.\end{aligned}\tag{25}$$

As to the electric boundary conditions, the conditions for the continuity of the tangential components of the electric field vector at the interface and the continuity of the normal components of the electric displacement can be stated as

$$\begin{aligned}\varphi^{(\mathrm{I})}&=\varphi^{(\mathrm{II})},\\ D_2^{(\mathrm{I})}&=D_2^{(\mathrm{II})}\end{aligned}\tag{26}$$

which amounts to two boundary conditions. Thus, there are six boundary conditions altogether for the general reflection and refraction problems.

Assuming that the incident wave is in medium I ($BaTiO_3$) $X_2 < 0$ with the propagation (incident) angle $\theta^{(0)}$ and the attenuation angle $\gamma^{(0)}$, propagating toward medium II ($Ba_2NaNb_5O_{15}$) with the interface on $X_2 = 0$. Here, the superscript (0) represents the incident wave. The incident waves can be either quasi-longitudinal (L) or quasi-transverse (T) waves in medium I.

In medium I, based on the assumption in Eq. (13), the reflected waves can be

$$u_s^{\mathrm{I(i)}}=c^{\mathrm{I(i)}}U_s^{\mathrm{I(i)}}\mathrm{e}^{j\left(k_m^{\mathrm{I(i)}}x_m-\omega t\right)},\quad \varphi_s^{\mathrm{I(i)}}=c^{\mathrm{I(i)}}\psi_s^{\mathrm{I(i)}}\mathrm{e}^{j\left(k_m^{\mathrm{I(i)}}x_m-\omega t\right)},\tag{27}$$

so are refracted waves in domain II

$$u_s^{\mathrm{II(i)}}=d^{\mathrm{II(i)}}U_s^{\mathrm{II(i)}}\mathrm{e}^{j\left(k_m^{\mathrm{II(i)}}x_m-\omega t\right)},\quad \varphi_s^{\mathrm{II(i)}}=d^{\mathrm{II(i)}}\psi_s^{\mathrm{II(i)}}\mathrm{e}^{j\left(k_m^{\mathrm{II(i)}}x_m-\omega t\right)}\tag{28}$$

where i indicates the wave mode, and c the reflection wave amplitude coefficients and d the refraction wave amplitude coefficients.

Substituting Eqs. (27)–(28) into the boundary condition, Eqs. (23) and (26) will lead to a set of nonlinear equations. Due to the phase match requirement on the interface of $X_2 = 0$, first we can obtain the general Snell's law for the inhomogeneous waves,

$$k_1^{(0)}=k_1^{(1)}=\cdots=k_1^{(S)},\tag{29}$$

alternatively

$$\begin{aligned}P^{(0)}\sin\theta^{(0)}&=P^{(1)}\sin\theta^{(1)}=\cdots=P^{(S)}\sin\theta^{(S)},\\ A^{(0)}\sin\left(\theta^{(0)}+\gamma^{(0)}\right)&=A^{(1)}\sin\left(\theta^{(1)}+\gamma^{(1)}\right)=\cdots=A^{(S)}\sin\left(\theta^{(S)}+\gamma^{(S)}\right),\end{aligned}\tag{30}$$

which can be illustrated in Fig. 2.

Equation (29) implies that the reflected and refracted waves have the same wave vector components parallel to the boundary with the incident wave. The normal component k_2 of the wave vector can be obtained by solving the dispersion Eq. (15) when k_1 is given, and the wave amplitude vector U_j can be acquired by Eq. (16) or (18).

Further, the phase match requirement on the boundary leads to the simultaneous equations about the wave reflection coefficient $c^{(\mathrm{r})}$ and refraction coefficient $d^{(\mathrm{r})}$:

$$\begin{aligned}G_i^{\mathrm{I(0)}}&=\sum_{r=1}^{S}\left(d^{(\mathrm{r})}G_i^{\mathrm{II(r)}}-c^{(\mathrm{r})}G_i^{\mathrm{I(r)}}\right),\\ H_j^{\mathrm{I(0)}}&=\sum_{r=1}^{S}\left(d^{(\mathrm{r})}H_j^{\mathrm{II(r)}}-c^{(\mathrm{r})}H_j^{\mathrm{I(r)}}\right),\\ L^{\mathrm{I(0)}}&=\sum_{r=1}^{S}\left(d^{(\mathrm{r})}L^{\mathrm{II(r)}}-c^{(\mathrm{r})}L^{\mathrm{I(r)}}\right)\end{aligned}\tag{31}$$

where

$$
\begin{aligned}
G_i^{\mathrm{I}(0)} &= I\left(\overset{\mathrm{o}}{C}_{i2kl}k_l U_k + e_{mi2}k_m \Psi\right)^{\mathrm{I}(0)}, \\
G_i^{\mathrm{I,II(r)}} &= I\left(\overset{\mathrm{o}}{C}_{i2kl}U_k k_l + e_{ki2}\Psi k_k\right)^{\mathrm{I,II(r)}}, \\
H_j^{\mathrm{I}(0)} &= I\left[U_1, U_2, \Psi\right]_j^{\mathrm{I}(0)}, \\
H_j^{\mathrm{I,II(r)}} &= I\left[U_1, U_2, \Psi\right]_j^{\mathrm{I,II(r)}}, \\
L^{\mathrm{I}(0)} &= I\left(e_{2kj}k_j U_k - \in_{2j} k_j \Psi\right)^{\mathrm{I}(0)}, \\
L^{\mathrm{I,II(r)}} &= I\left(e_{2kj}k_j U_k - \in_{2j} k_j \Psi\right)^{\mathrm{I,II(r)}}.
\end{aligned} \tag{32}
$$

Apparently, there are six equations in the boundary conditions of Eq. (31), which require six reflected and refracted wave modes at the interface inherently. In the two-dimensional case, there are only two bulk wave modes in each medium, and thus seemingly there emerges a mismatching problem in the linear piezoelectricity theory due to the quasi-static approximation of the electric field. As shown in Sect. 4, the inhomogeneous wave theory can allow a reflected or refracted surface wave mode by obeying Snell's law. Accordingly, the additional wave mode can be described in the same way as those elastic wave modes in Eqs. (2)–(28). Thus, Eq. (31) becomes resolved mathematically. Rather than the regular surface wave, the reflected or refracted surface wave satisfies the boundary condition with other bulk waves together.

Based on the reflection and refraction theory in Eq. (29) or (30), the amplitude coefficients of Eqs. (27) and (28) can be obtained in the following steps: first, specify the propagation angle θ, attenuation angle γ and angular velocity $\mathbf{\Omega}$ and then substitute them into Eqs. (20) and (21) to obtain $(P,\ A)$, wave vector k_i and its component k_1 parallel to the boundary according to Eq. (20). Since all the reflection waves obey Snell's law, viz. Eq. (29), all the reflected and refracted waves share the same K_1 with the incident wave. Substituting k_1 into Eq. (15) leads to an equation in k_2,

$$
\det \Lambda\left(k_2; k_1, \omega, \mathbf{\Omega}\right) = 0, \tag{33}
$$

which can be solved for k_2 without any difficulty given k_1, ω and $\mathbf{\Omega}$. The conditions to determine whether the wave vector k_2 belongs to the reflection domain are

$$
\begin{cases} \mathrm{Re}[k_2] < 0 \\ \mathrm{Im}[k_2] \leq 0 \end{cases} \quad \text{for reflected waves} \tag{34}
$$

and

$$
\begin{cases} \mathrm{Re}[k_2] > 0 \\ \mathrm{Im}[k_2] \geq 0 \end{cases} \quad \text{for refracted waves.} \tag{35}
$$

Thus, all the wave vectors including incident, reflected and refracted waves $\mathbf{k}^{(0)}, \mathbf{k}^{\mathrm{I}(1)}, \ldots, \mathbf{k}^{\mathrm{I}(S)}$ $\mathbf{k}^{\mathrm{II}(1)}, \ldots, \mathbf{k}^{\mathrm{II}(S)}$ can be found, and their polarization of U_{i} can be determined by Eq. (18). Finally, one can solve the amplitude coefficients $c^{(\mathrm{i})}$ and $d^{(\mathrm{j})}$: $i, j = 1 \ldots S$ by the boundary conditions specified in Eq. (31).

Once all reflected and refracted waves are determined, they should be validated to ensure that the energy of incident waves is equal to the energy sum of reflected and refracted waves, i.e., the sum of energy flux component along the normal direction of the boundary should be conserved,

$$
\sum_{i=1}^{S} P_2^{(i)} = P_2^{(0)}, \tag{36}
$$

and

$$
P_i = -\sigma_{ji}\dot{u}_j + \varphi\dot{D}_i = -\overset{\mathrm{o}}{C}_{jikl}\varepsilon_{k,l}\dot{u}_j + \varphi\dot{D}_i \tag{37}
$$

Table 1 Material properties of $BaTiO_3$ (indicated by Ti) and $Ba_2NaNb_5O_{15}$ (indicated by Na) crystals

Elasticity tensor C_{ij} (GPa)	C_{11}	C_{22}	C_{55}
$BaTiO_3$	150.4	146.0	44.0
$Ba_2NaNb_5O_{15}$	239	135	66
Piezoelectricity tensor e_{ij} (C/m^2)	e_{22}	e_{21}	e_{15}
$BaTiO_3$	17.50	−4.35	11.40
$Ba_2NaNb_5O_{15}$	4.3	−0.4	2.8
Normalized permittivity tensor ϵ_{ij}/ϵ_0	ϵ_{11}/ϵ_0	ϵ_{22}/ϵ_0	
$BaTiO_3$	115.0	8.4	
$Ba_2NaNb_5O_{15}$	222.0	32.0	
Vacuum permittivity ϵ_0 (F/m)	8.854×10^{-12}		
Density ρ (kg/m^3)	($BaTiO_3$)		5700
	($Ba_2NaNb_5O_{15}$)		5300

where $P_2^{(i)}$ is the energy flux component of reflection or refraction wave along the normal direction to the boundary [31], and i indicates the i-th wave mode. Normalizing Eq. (36) with respect to the incident wave yields the dimensionless energy conservation equation

$$\sum_{i=1}^{S} \kappa^{(i)} = 1 \tag{38}$$

where $\kappa^{(i)} = P_2^{(i)}/P_2^{(0)}$ is the energy coefficient of the i-th wave mode.

4 Results and discussion

4.1 WAVE modes in a two-dimensional infinite medium

In order to conduct the investigation of wave reflection and refraction between the piezoelectric crystals, we should know the wave vectors of an infinite piezoelectric crystal. Consider two typical piezoelectric crystals of $BaTiO_3$ and $Ba_2NaNb_5O_{15}$ with material properties given in Table 1 [30,33].

According to the inhomogeneous wave theory outlined in the previous section, the wave velocities of two bulk waves, quasi-longitudinal (L) and quasi-transverse (T) waves, are calculated, given θ, γ, $\mathbf{\Omega}$, initial stresses $\boldsymbol{\sigma}_{il}^0$ and the circular frequency $\omega = 2\pi \times 10^6\ \mathrm{s}^{-1}$.

Let us start from examining the bulk waves that lie on the X_1X_2, on which the piezoelectric planes rotate about X_3 (thus, $\mathbf{\Omega} = \Omega_3\mathbf{E}_3$). According to Eq. (12) and inhomogeneous wave solution in Sect. 3, there are two bulk waves in the piezoelectric plane: one quasi-longitudinal wave indicated by **L**, and the other is the quasi-transverse wave **T**.

4.1.1 The bulk waves of $BaTiO_3$

(i) Quasi-longitudinal wave: **L**

Because there is no viscous item considered in the governing equations, namely Eq. (10) or (12), the attenuation angle γ is found to be ignorable to the wave velocity. Figure 3 depicts the quasi-longitudinal wave velocities of varying angular velocities in $BaTiO_3$, which significantly affect the wave velocity. Because of the anisotropic property of the piezoelectric body, the wave velocity performs differently at different propagation angle. Obviously, the relationship between velocity and angular velocity is not linearly dependent. For making clearer the relationship between phase velocity and rotation velocity, we present Fig. 4 showing that there exists a singular point when rotation velocity is equal to the wave frequency; the velocity curve is characterized by an abrupt change near the singular point. Before this point, the wave velocity is increasing with the rotation velocity; surpassing this point, the wave velocity is declining sharply. At this singular point, no quasi-longitudinal wave can be obtained for any propagation angle θ as seen in Fig. 3.

Further, the influence of the initial stresses on wave velocities is examined with the velocity variation ratio from natural states to stressed state as indicated by $\left(\Delta v/v_{\text{natural}}\right)\%$ on the right vertical axis depicted in Fig. 4. $\Delta v = v_{\text{stressed}} - v_{\text{natural}}$ and v_{natural} is the state without initial stresses. The ratio curve reveals that

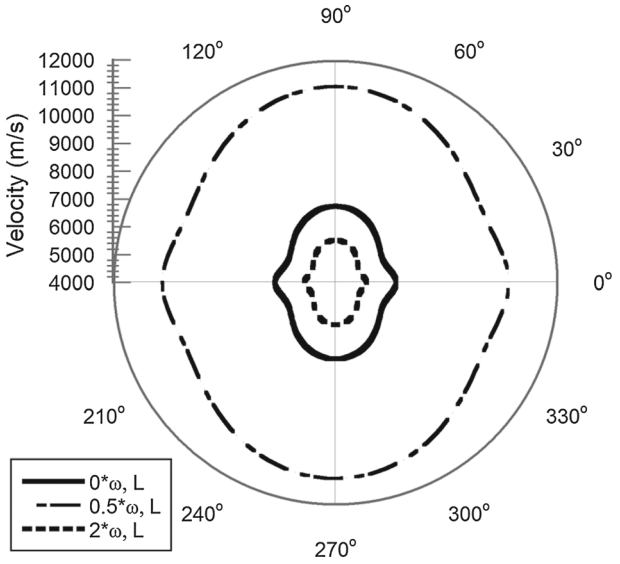

Fig. 3 Phase velocity of the quasi-longitudinal wave (indicated by L) versus propagation angle θ ranging from 0° to 360° with $\gamma = 0, \sigma_{11} = \sigma_{22} = 10^9$ Pa and varied angular velocity Ω_3 (0, 0.5, 1 or 2 represent the ratios between Ω_3 and wave frequency ω) in case of the two-dimensional piezoelectric crystal of $BiTiO_3$

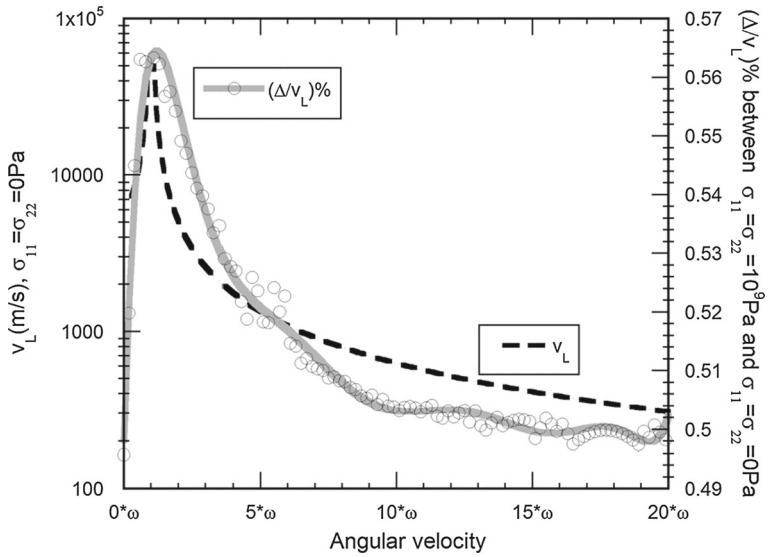

Fig. 4 Phase velocity of the quasi-longitudinal wave (indicated by L), velocity variation ratio versus angular velocity Ω_3 for $\theta = 45°$ and $\gamma = 0$ in case of the two-dimensional piezoelectric crystal of $BiTiO_3$

the velocity has a weak dependence on the initial stresses. All the ratios are below 1 %. Besides, the ratio is related to the angular velocity and gets its maximum value at about the singular point (when the angular velocity is equal to the wave frequency). In the angular velocity's range between $0^*\omega$ and $1^*\omega$, the variation is large and away from the singular point, and the curve becomes stable.

(ii) Quasi-transverse wave: **T**

Figure 5 presents the dependency of the quasi-transverse wave velocity on the propagation angle. Other than the L wave, there is no singular point for T wave velocity, which is approximately decreasing monotonously with the angular velocity as seen in Fig. 6. Likewise, it is found that the attenuation angle γ almost does not influence **T**'s wave velocity. The initial stresses also show slight contribution to the velocity variation ratio below 1 % and gets to its bottom, when the angular velocity is equal to the wave frequency.

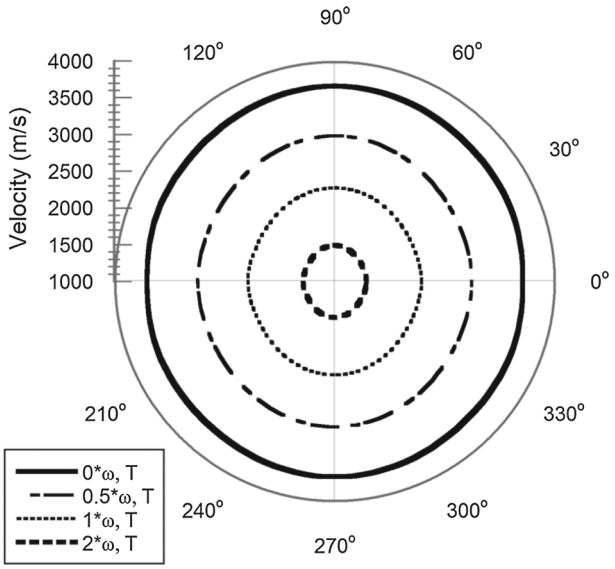

Fig. 5 Phase velocity of the quasi-transverse wave (indicated by *T*) versus propagation angle θ ranging from 0° to 360° with $\gamma = 0$, $\sigma_{11} = \sigma_{22} = 10^9$ Pa and varied angular velocity Ω_3 (0, 0.5, 1 or 2 represent the ratios between Ω_3 and wave frequency ω) in case of the two-dimensional piezoelectric crystal of $BiTiO_3$

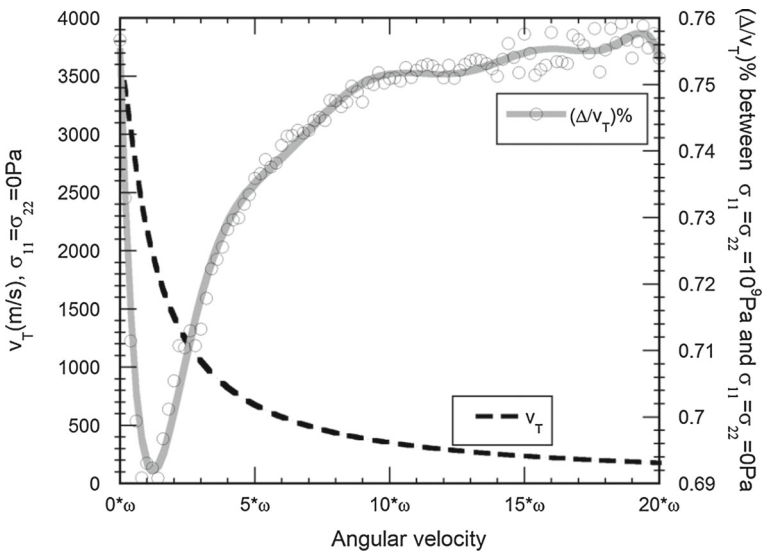

Fig. 6 Phase velocity of the quasi-transverse wave (indicated by *T*), velocity variation ratio versus angular velocity Ω_3 for $\theta = 45°$ and $\gamma = 0$ in case of the two-dimensional piezoelectric crystal of $BiTiO_3$

4.1.2 The bulk waves of $Ba_2NaNb_5O_{15}$

(i) Quasi-longitudinal wave: **L**

Likewise, we investigate the bulk wave of $Ba_2NaNb_5O_{15}$ and obtain similar results as $BiTiO_3$. The relationships between the quasi-longitudinal wave velocities and propagation angle/angular velocity are plotted respectively in Figs. 7 and 8. The figures show that the singular point of the equality between the angular velocity and wave frequency exists for the quasi-longitudinal wave, close to which the velocity has a sharp modification, at which the velocity cannot be obtained. Away from this point, the velocities drop quickly.

Figure 8 shows the phase velocity of the quasi-longitudinal wave (indicated by **L**), velocity variation ratio versus angular velocity Ω_3 for $\theta = 45°$ and $\gamma = 0$ in case of the two-dimensional piezoelectric crystal of

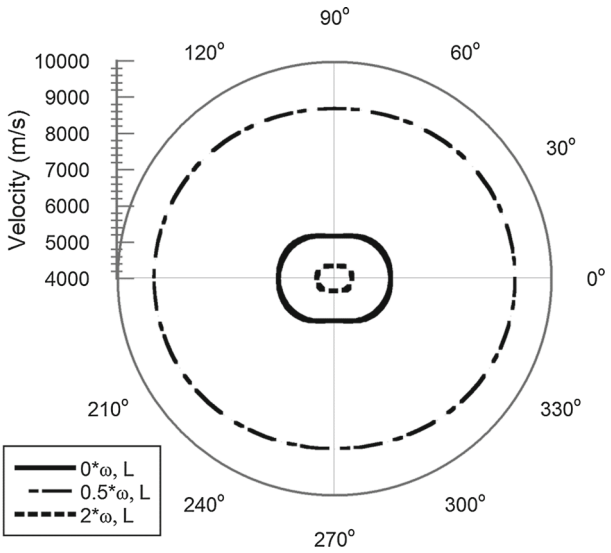

Fig. 7 Phase velocity of the quasi-longitudinal wave (indicated by L) versus propagation angle θ ranging from 0° to 360° with $\gamma = 0$, $\sigma_{11} = \sigma_{22} = 10^9$ Pa and varied angular velocity Ω_3 (0, 0.5, 1 or 2 represent the ratios between Ω_3 and wave frequency ω) in case of the two-dimensional piezoelectric crystal of $Ba_2NaNb_5O_{15}$

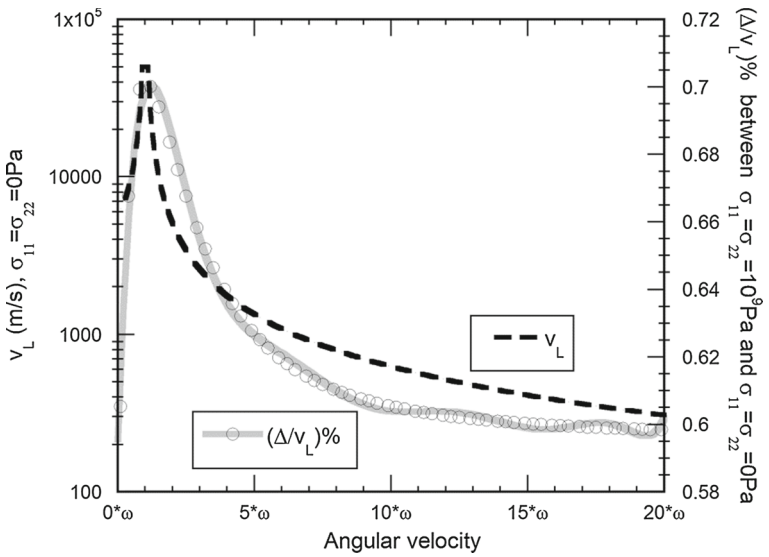

Fig. 8 Phase velocity of the quasi-longitudinal wave (indicated by L), velocity variation ratio versus angular velocity Ω_3 for $\theta = 45°$ and $\gamma = 0$ in case of the two-dimensional piezoelectric crystal of $Ba_2NaNb_5O_{15}$

$Ba_2NaNb_5O_{15}$. Also, the initial stresses have slight impact on the velocity and at the same time are associated with the angular velocity whose trend is of the kind of the velocity curve indicated on the left vertical axis.

(ii) Quasi-transverse wave: **T**

Distinctly, the quasi-transverse wave T does not have a singular point in the angular velocity, which can be revealed in Fig. 10. In addition, the velocity declines with the angular velocity, i.e., in Figs. 9 and 10. The initial stresses still play a small role in the wave velocity, and the effects are changing with the angular velocity.

4.2 The wave reflection/refraction over the boundary interface

Considering the boundary condition in Eq. (25), we can see that there are six equations. At the same time, the former section indicates that there are two bulk wave modes in each two-dimensional piezoelectric crystal in

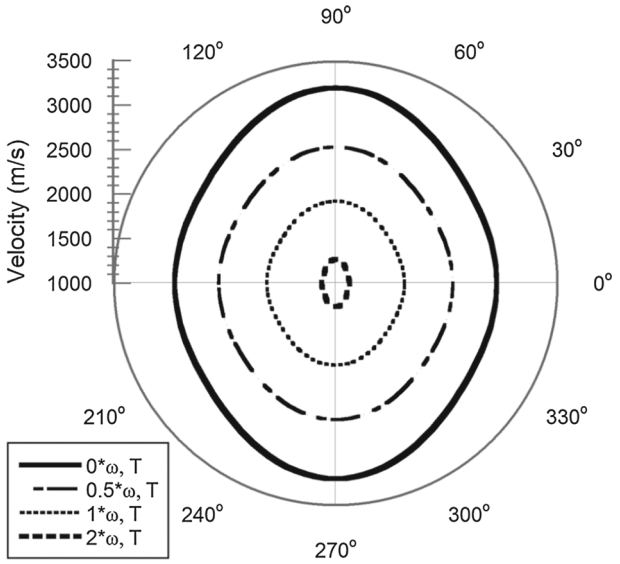

Fig. 9 Phase velocity of the quasi-transverse wave (indicated by T) versus propagation angle θ ranging from 0° to 360° with $\gamma = 0$, $\sigma_{11} = \sigma_{22} = 10^9$ Pa and varied angular velocity Ω_3 (0, 0.5, 1 or 2 represent the ratios between Ω_3 and wave frequency ω) in case of the two-dimensional piezoelectric crystal of $Ba_2NaNb_5O_{15}$

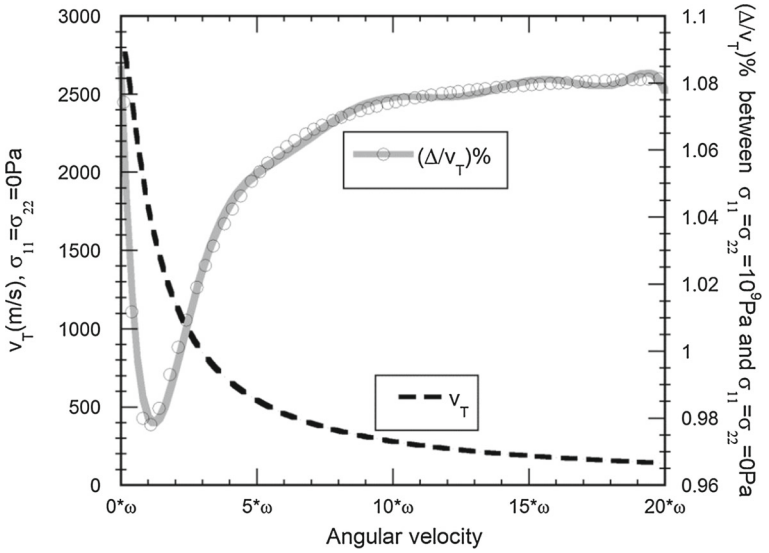

Fig. 10 Phase velocity of quasi-transverse wave (indicated by T), velocity variation ratio versus angular velocity Ω_3 for $\theta = 45°$ and $\gamma = 0$, in case of the two-dimensional piezoelectric crystal of $Ba_2NaNb_5O_{15}$

the biaxial stressed states. It seemingly produces a contradictory situation of the inequality between equation number and the wave modes, while it can be resolved in the framework of inhomogeneous wave theory as revealed later.

Considering that the angular velocity is below the wave frequency, hereafter we will handle computation examples, typically $\Omega_3 = 0.5\omega$ and stressed state $\sigma_{11} = \sigma_{22} = 10^9$ Pa.

4.2.1 Incident wave of wave mode **L**

Assume the incident wave is the quasi-longitudinal wave propagating in the half plane of $BiTiO_3$. Definitely, there will be two reflected bulk wave modes within it and two refracted bulk wave modes in the half plane $Ba_2NaNb_5O_{15}$ as outlined previously. In addition to the normal L and T wave modes, the computation results also exhibit that there exists the reflected surface wave always moving over the interface for all incident angles

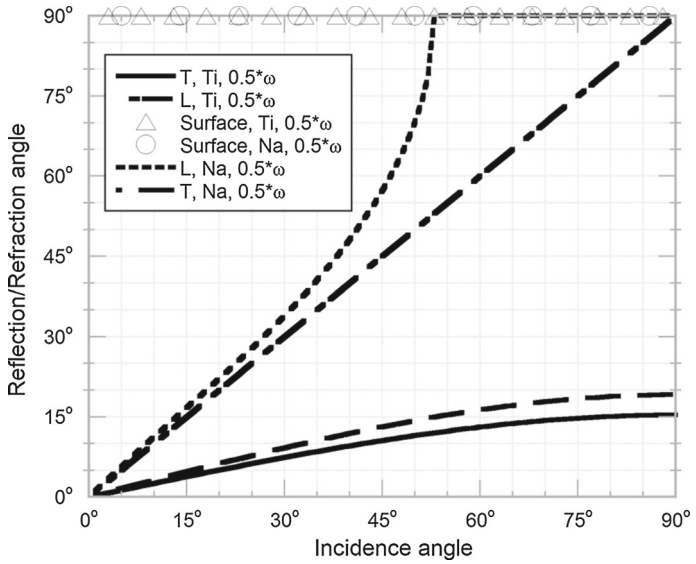

Fig. 11 Reflection and refraction angle versus incidence angle θ. The incident wave is L mode with the attenuation angle $\gamma = 0$, angular velocity $\Omega_3 = 0.5^*\omega$, $\sigma_{11} = \sigma_{22} = 10^9$ Pa

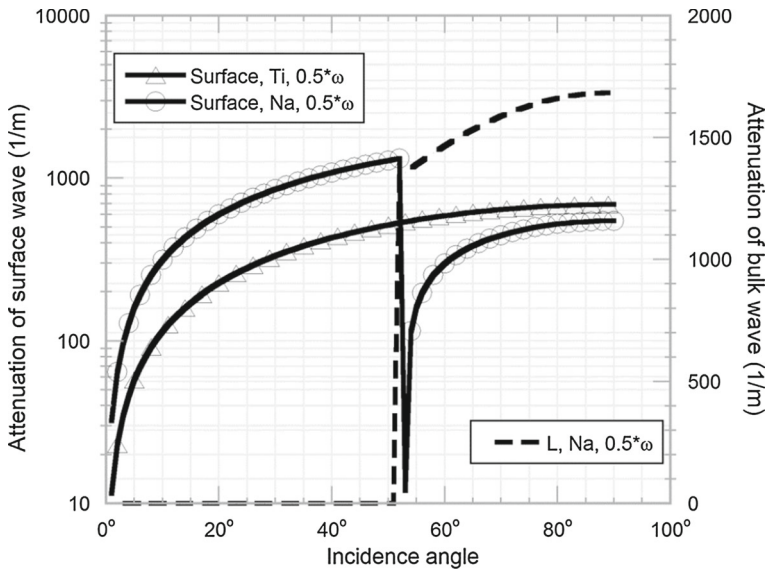

Fig. 12 Reflected/refracted wave attenuations versus propagation angle θ. The incident wave is L mode with the attenuation angle $\gamma = 0$, angular velocity $\Omega_3 = 0.5^*\omega$, $\sigma_{11} = \sigma_{22} = 10^9$ Pa

ranging from 0° to 90° and vanishing quickly perpendicular to the interface, which can be called surface wave mode accordingly.

Figure 11 shows the variation of reflection/refraction angles of three reflected waves in $BaTiO_3$ and three refracted waves in $Ba_2NaNb_5O_{15}$ as functions of incident angle θ, the attenuation angle $\gamma = 0$, angular velocity $\Omega_3 = 0.5^*\omega$, and biaxial stress $\sigma_{11} = \sigma_{22} = 10^9$ Pa. As expected, the reflection/refraction angle obeys Snell's law and is defined as arctan[Re(k_1)/Re(k_2)], which can be associated with velocity plots in Figs. 3, 4, 5, 6, 7, 8, 9 and 10. Evidently, fast velocity implies large reflection/refraction angle, vice versa. A larger refraction angle occurs in case of refracted L wave in $Ba_2NaNb_5O_{15}$, and it comes to move parallel to the interface from about 50° of the incidence angle. At the same time, its attenuation has an abrupt change from zero as seen from Fig. 12. Meanwhile, the refracted wave of T in Na is below the incident angle and so is the reflected T wave in $BiTiO_3$.

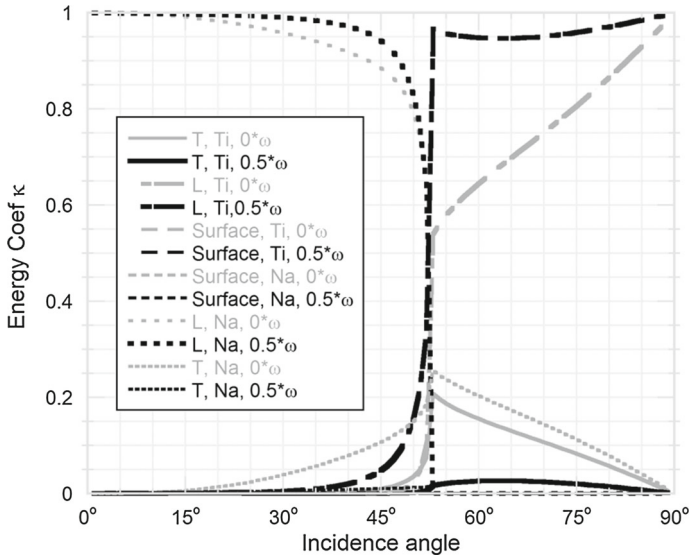

Fig. 13 Variations of energy coefficients with incident angle. The incident wave is L mode with the attenuation angle $\gamma = 0$, angular velocity $\Omega_3 = 0, 0.5^*\omega$, $\sigma_{11} = \sigma_{22} = 10^9$ Pa

Notably, there is a reflected wave in $BiTiO_3$ and a refracted wave $Ba_2NaNb_5O_{15}$ both always propagating parallel to the interface. Further, Fig. 12 presents the attenuations of the reflection surface wave and refraction surface wave perpendicular to the interface, respectively, which are always nonzero at any incidence angle. Meanwhile, the attenuation rises with the incidence angle, and the angular velocity can affect the attenuation as well. Thus, it is reasonable to call these waves as surface mode according to their propagation directions and attenuations.

Finally, it should be remarked that the initial stresses could change the reflection/refraction angle somehow considering their effects on wave velocities is slight, while the angular velocity has a bigger impact, which can be interpreted by their association with wave velocity discussed above.

From the point of view of power flow, the above-mentioned wave field should follow the well-known conservation of energy flux requiring that the sum of energy coefficients is unity, which can be utilized as a validation method on the analysis and a tool to estimate whether the reflected and refracted waves are right physically.

The energy transfer between the incident and reflected/refracted waves is shown in Fig. 13 at distinct angular velocities $\Omega_3 = 0, 0.5^*\omega$, respectively. Evidently, both results satisfy the energy conservation law. At the normal incidence, there is only a refracted L Na wave. As the incident angle increases, other wave modes start to gain energy gradually. At the critical angle of 53°, there is an abrupt change in energy distribution, where the QL Na wave drops to zero quickly, which can be linked to its attenuation as seen in Fig. 12. At the same time, the reflected L Ti wave becomes the dominant wave mode. In all cases, the energy fluxes of the surface waves are almost zero, which indicates that the introduction of the reflected/refracted surface wave modes does not modify the energy law between the incident, reflected and refracted waves. In addition, the figure shows that the energy coefficients also depend on the angular velocity which makes the energy conversion between different wave modes more sharply than the nonrotating case.

4.2.2 Incident wave of wave mode **T**

Here we turn to investigate the reflected and refracted waves incurred by the incident quasi-transverse wave (**T** mode). Similar to the incident **L** wave, there are six reflected wave modes comprising **L** and **T** bulk wave modes as well as the surface wave (**Surface**) both in $BiTiO_3$ and in $Ba_2NaNb_5O_{15}$.

Figure 14 shows the variation of reflection angles of three reflected waves (**L**, **T** bulk wave modes and surface wave (**Surface**)) as functions of the incident angle θ in the case of attenuation angle $\gamma = 0$, $\Omega_3 = 0.5^*\omega$ and biaxial stressed state. It is observed that the reflection angle of the **L** wave is always larger than the **T** wave because the **L** wave travels faster than the **T** wave. Apparently, the **Surface** wave moves at the X_1X_3 plane, weakening perpendicular to the plane in any incidence angle as depicted in Fig. 15. The reflected L

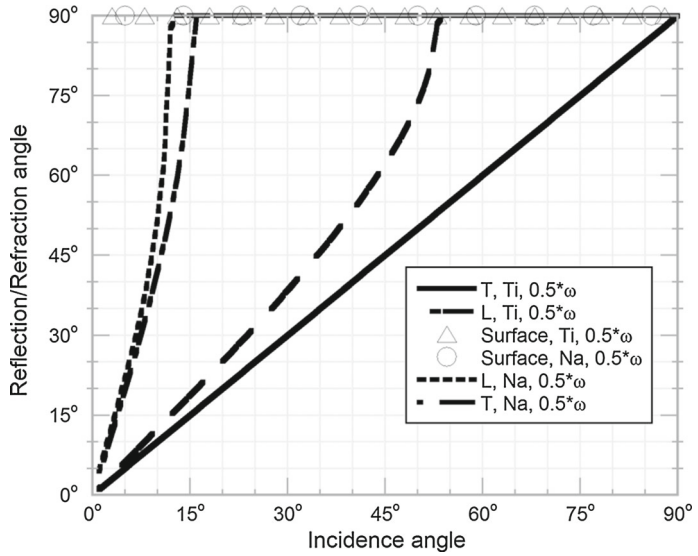

Fig. 14 Reflection and refraction angle versus incidence angle θ. The incident wave is T mode with the attenuation angle $\gamma = 0$, angular velocity $\Omega_3 = 0.5^*\omega$, $\sigma_{11} = \sigma_{22} = 10^9$ Pa

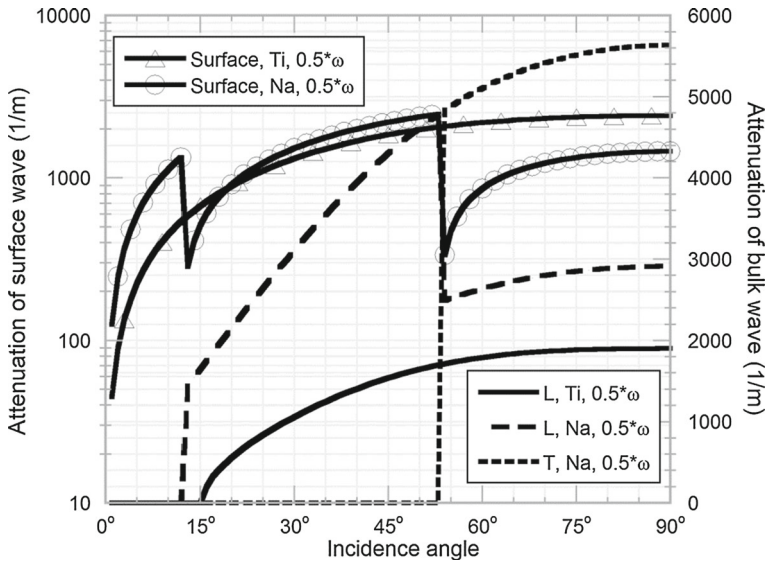

Fig. 15 Reflected/refracted wave attenuations versus propagation angle θ. The incident wave is T mode with the attenuation angle $\gamma = 0$, angular velocity $\Omega_3 = 0.5^*\omega$, $\sigma_{11} = \sigma_{22} = 10^9$Pa

wave in $BiTiO_3$ from about 15° acts the same way as the surface wave due to its propagation direction in Fig. 14 and its attenuation in Fig. 15, and so do the refracted L and T waves in $Ba_2NaNb_5O_{15}$ as shown in Fig. 14. Obviously, the attenuation of reflected L waves jumps from zero to a large number. The rotation effects on the wave velocity are depicted in Fig. 3, which shows the phase velocity of a quasi-longitudinal wave (indicated by **L**) versus propagation angle θ ranging from 0° to 360° with $\gamma = 0, \sigma_{11} = \sigma_{22} = 109$ Pa and varied angular velocity Ω_3 (0, 0.5, 1 or 2 represent the ratios between Ω_3 and wave frequency ω) in case of the two-dimensional piezoelectric crystal of $BiTiO_3$. Figure 10 shows the phase velocity of the quasi-transverse wave (indicated by T), velocity variation ratio versus angular velocity Ω_3 for $\theta = 45°$ and $\gamma = 0$, in case of the two-dimensional piezoelectric crystal of ($Ba_2NaNb_5O_{15}$); the angular velocity can also play a role in the reflected and refracted angles.

Figure 14 presents the nonzero attenuation of reflected and refracted waves, which should be compared with the angle figure of Fig. 13. It is observed that when the abrupt change of wave attenuation is associated

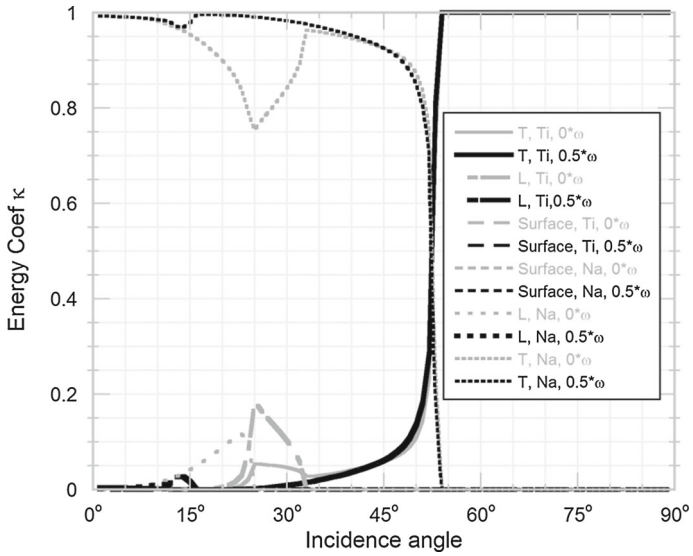

Fig. 16 Variations of energy coefficients with incidence angle. The incident wave is T mode with the attenuation angle $\gamma = 0$, angular velocity $\Omega_3 = 0, 0.5^*\omega$, $\sigma_{11} = \sigma_{22} = 10^9$ Pa

with its propagation angle along the interface, the surface wave attenuations are always high in any incidence angle.

The energy coefficients between the incident and reflected/refracted waves in Fig. 16 evidently show the energy conservation law. Starting at the normal incidence, there are three reflected waves in $BiTiO_3$ including **T Ti**, **L Ti** and **Surface Ti** waves and three refracted waves in $Ba_2NaNb_5O_{15}$, i.e., **T Na, L Na** and **Surface Na** waves. The energy of the incident wave is transferred into the refracted T Na mode wave nearly 100 % at zero incidence angle. As the incidence angle increases, the other wave modes, L Ti, L Na, T Ti, start to be excited. As the incidence angle approaches to and exceeds some points, the reflected L Ti wave at roughly 25° and refracted L Na wave at roughly 35 degrees become the surface wave (propagating parallel to the interface, see Fig. 14), and its attenuation increases dramatically as shown Fig. 15. The energy associated with the reflected L Na wave mode reduces to almost zero. Similar phenomena occur for the refracted T Na wave at the corresponding critical angle 56°. After 56°, the T Ti wave takes over all the incident energy. Physically, it implies that there will exist only a Q Ti wave beyond the critical incident angle of 56°. There is almost no energy associated with two surface waves Surface Ti and Surface Na in all cases.

Figure 16 shows that the summation of the energy coefficients of all these waves equals almost unity in the case of angular velocity $\Omega_3 = 0$ or $0.5^*\omega$. This indicates that the model is reasonable in physics, and the introduction of the surface wave does not violate the energy transmission between the incident and reflected/refracted waves while avoiding the mathematical difficulty in solving the boundary problem of quasi-static wave reflection/refraction in a piezoelectric medium. Thus, the inhomogeneous wave is an advisable approach in dealing with the inconsistent boundary condition problem caused by the quasi-static approximation in the electric field. On account of the small effects of initial stresses on velocity, the energy curves of natural state and stressed state are quite similar.

5 Conclusions

In this paper, we developed an approach to deal with the wave reflection and refraction problem in two half planes of rotating and biaxial stressed piezoelectric crystals using the inhomogeneous wave theory. The piezoelectric crystals are taken to be at equilibrium with initial biaxial stresses. Hence, the dynamics is examined under the assumption of a small motion superimposed to the equilibrium configuration. In contrast to the initial stresses shown in the computation results, the presence of the Coriolis and centrifugal acceleration demonstrates more obvious influence upon the wave propagation and reflection/refraction, i.e., the wave velocities and attenuations, the angles of the reflected/refracted bulk waves and energy ratio coefficients. The examples show that there is a singular point when angular velocity equals the wave frequency, close to which

the quasi-longitudinal wave shows an abrupt change, and at which the quasi-longitudinal wave cannot be obtained. Instead, the quasi-transverse wave does not have such a singular point in case of rotation. Besides, no quasi-longitudinal wave can be reflected or refracted whatever the incident wave mode is at the point. Apart from this point, there are two reflected and two refracted bulk wave modes as well as the incurred surface wave modes to address the issue of the elastic and electric boundary conditions mismatching the number of wave modes due to the quasi-static assumption in the linear piezoelectricity theory. Unlike the regular surface wave, the pseudo-surface wave satisfies the boundary conditions together with the incident and reflected waves. The analysis results also indicate that the reflected and refracted bulk waves can turn into the type of surface wave at some incidence angle in the case of incident quasi-longitudinal and quasi-transverse waves. Rather than the rotation, the initial stresses show slight effects on the waves. The methodology and computation results presented in this paper may be helpful in the application of oscillators and mechanical sensors or in designing the controlling devices of acoustoelectronics from the practical point of view.

Acknowledgments The support of this research by a grant of HPU 72515/468 is gratefully acknowledged. The authors are indebted to the reviewers for valuable suggestions.

References

1. Huston, R.L.: Wave propagation in rotating elastic media. AIAA J. **2**, 575–576 (1964)
2. Huston, R.L.: In-plane vibration of spinning disks. AIAA J. **3**, 1519–1520 (1965)
3. Schoenbe, M., Censor, D.: Elastic-waves in rotating media. Q. Appl. Math, **31**, 115–125 (1973)
4. Lao, B.Y.: Gyroscopic effect in surface acoustic waves. In: MacAvoy, B.R. (ed.) IEEE Ultrasonics Symposium, pp. 687–691. Boston, MA (1980)
5. Roy Choudhuri, S.K.: Electro-magneto-thermo-elastic plane waves in rotating media with thermal relaxation. Int. J. Eng. Sci. **22**, 519–530 (1984)
6. Bera, R.K.: Propagation of waves in random rotating infinite magneto-thermo-visco-elastic medium. Comput. Math. Appl. **36**, 85–102 (1998)
7. Wauer, J.: Waves in rotating conducting piezoelectric media. J. Acoust. Soc. Am. **106**, 626–636 (1999)
8. Destrade, M., Saccomandi, G.: Some results on finite amplitude elastic waves propagating in rotating media. Acta. Mech. **173**, 19–31 (2004)
9. Destrade, M.: Surface acoustic waves in rotating orthorhombic crystals. Proc. R. Soc. Lond. Ser. A Math. Physical and Eng. Sci. **460**, 653–665 (2004)
10. Ting, T.C.T.: Surface waves in a rotating anisotropic elastic half-space. Wave Motion **40**, 329–346 (2004)
11. Auriault, J.L.: Body wave propagation in rotating elastic media. Mech. Res. Commun. **31**, 21–27 (2004)
12. Auriault, J.-L.: Acoustics of rotating deformable saturated porous media. Transp. Porous Med. **61**, 235–237 (2005)
13. Yang, J.s.: A review of analyses related to vibrations of rotating piezoelectric bodies and gyroscopes. IEEE Trans. Ultrason. Ferroelectr. Freq. Control **52**, 698–706 (2005)
14. Singh, J., Tomar, S.K.: Plane waves in a rotating micropolar porous elastic solid. J. Appl. Phys. **102**, 074906–074907 (2007)
15. Sharma, J.N., Grover, D.: Body wave propagation in rotating thermoelastic media. Mech. Res. Commun. **36**, 715–721 (2009)
16. Kumar, R. Rupender: Effect of rotation in magneto-micropolar thermoelastic medium due to mechanical and thermal sources. Chaos Solitons Fractals **41**, 1619–1633 (2009)
17. Biryukov, S.V., Schmidt, H., Weihnacht, M.: Gyroscopic effect for SAW in common piezoelectric crystals. In: Pappalardo M. (ed.) Ultrasonics Symposium (IUS), 2009 IEEE International, pp. 2133–2136. Rome, Italy (2009)
18. Sharma, J.N., Grover, D., Kaur, D.: Mathematical modelling and analysis of bulk waves in rotating generalized thermoelastic media with voids. Appl. Math. Model. **35**, 3396–3407 (2011)
19. Wegert, H., Reindl, L.M., Ruile, W., Mayer, A.P.: On the Coriolis effect in acoustic waveguides. J. Acoust. Soc. Am. **131**, 3794–3801 (2012)
20. Prasad, R., Mukhopadhyay, S.: Effects of rotation on harmonic plane waves under two-temperature thermoelasticity. J. Therm. Stresses **35**, 1037–1055 (2012)
21. Kothari, S., Mukhopadhyay, S.: Study of harmonic plane waves in rotating thermoelastic media of type III. Math. Mech. Solids **17**, 824–839 (2012)
22. Abd-Alla, A.M., Yahya, G.A.: Thermal stresses in infinite circular cylinder subjected to rotation. Appl. Math. Mech. Engl. Ed. **33**, 1059–1078 (2012)
23. Yuan, X., Chen, S.: The inhomogeneous waves in a rotating piezoelectric body. Sci. World J. **2013**, 8 (2013)
24. Zhou, Y.H., Jiang, Q.: Effects of Coriolis force and centrifugal force on acoustic waves propagating along the surface of a piezoelectric half-space. Z. Angew. Math. Phys. **52**, 950–965 (2001)
25. Yuan, X.: Inhomogeneous wave reflection in a rotating piezoelectric body. Acta. Mech. **226**, 811–827 (2015)
26. Pao Y., H., Gamer, U.: Acoustoelastic waves in orthotropic media. J. Acoust. Soc. Am. **77**, 806–812 (1985)
27. Simionescu-Panait, O.: Energy estimates for Love wave in a pre-stressed layered structure. Ann. Univ. Buchar. (Math. Ser.) **4**, 229–241 (2013)
28. Gandhi, N., Michaels, J.E., Lee, S.J.: Acoustoelastic Lamb wave propagation in biaxially stressed plates. J. Acoust. Soc. Am. **132**, 1284–1293 (2012)
29. Kuang, Z.-B.: Theory of Electroelasticity. Shanghai Jiao Tong University Press, Springer-Verlag, Shanghai, Berlin Heidelberg (2014)

30. Kuang, Z.B., Yuan, X.: Reflection and transmission of waves in pyroelectric and piezoelectric materials. J. Sound Vib. **330**, 1111–1120 (2011)
31. Yuan, X.: The energy process of pyroelectric medium. J. Therm. Stresses **33**, 413–426 (2010)
32. Yuan, X., Kuang, Z.: The inhomogeneous waves in pyroelectrics. J. Therm. Stresses **33**, 172–186 (2010)
33. Yuan, X., Zhu, Z.H.: Reflection and refraction of plane waves at interface between two piezoelectric media. Acta. Mech. **223**, 2509–2521 (2012)
34. Goldstein, H., Poole, C.P., Safko, J.L.: Classical Mechanics. Addison-Wesley, San Francisco (2002)